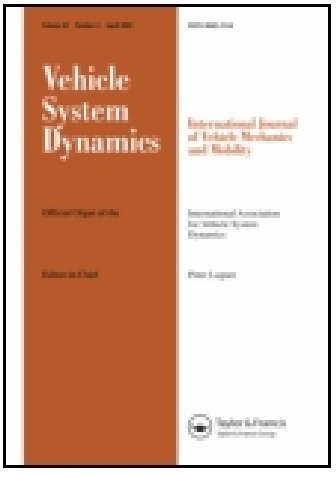

Vehicle System Dynamics: International Journal of Vehicle Mechanics and Mobility

Publication details, including instructions for authors and subscription information:
http://www.tandfonline.com/loi/nvsd20

Fault detection of vehicle suspension system using wavelet analysis

Shahram Azadi [a] & Abbas Soltani [a]

[a] Faculty of Mechanical Engineering , Khajeh Nasireddin Tousi University of Technology , Tehran, Iran

Published online: 18 Mar 2009.

To cite this article: Shahram Azadi & Abbas Soltani (2009) Fault detection of vehicle suspension system using wavelet analysis, Vehicle System Dynamics: International Journal of Vehicle Mechanics and Mobility, 47:4, 403-418

To link to this article: http://dx.doi.org/10.1080/00423110802094298

Vehicle System Dynamics
Vol. 47, No. 4, April 2009, 403–418

Taylor & Francis
Taylor & Francis Group

Fault detection of vehicle suspension system using wavelet analysis

Shahram Azadi* and Abbas Soltani

Faculty of Mechanical Engineering, Khajeh Nasireddin Tousi University of Technology, Tehran, Iran

(*Received 7 September 2007; final version received 1 April 2008*)

This paper presents a method based on continuous wavelet transform to detect the faults of vehicle suspension systems. The Morlet wavelet functions are employed to approach the natural frequencies of the system and the frequency components of the signal with relative maximum energy. To evaluate our method, we use a full vehicle dynamic model which has been simulated in ADAMS/CAR and validated by laboratory test results. The suspension faults have been considered due to the damage of shock absorbers (dampers) and upper damper bushings (UDBs) and assumed as the decrease in damping force and loose joints, respectively. In this paper, the incapability of the spectral analysis by using fast Fourier transform in analysis of the signals is revealed through applying the inputs that include transient characteristics and then wavelet transform employed to achieve more proper results. A swept frequency is applied as an input to the wheels that simulates the road irregularities. After detection of faulty sections of the system using signal energy distribution, the defects of damper and UDBs are distinguished from each other through observing the changes of natural frequencies and corresponding energy amplitudes.

Keywords: continuous wavelet transform; Morlet wavelet; suspension system; fault detection

1. Introduction

The measurement and analysis of vibratory signals is one of the most useful methods for fault detection in mechanical systems and very useful information can be obtained about the performance of the systems by using this method.

These methods have been used and have made progress in the successive years. After introducing the fast Fourier transform (FFT), the spectral analysis became one of the most efficient methods to analyse vibration signals of the dynamic systems and it is considered as a powerful method yet.

Many research studies have been conducted on this subject up to now. McFadden used vibration analysis to identify the local defects of the gears and roller bearings [1]. This study and other performed studies on the fault detection of the mechanical systems and monitoring were mainly based on the spectral analysis methods. Nevertheless, the spectral analysis is incapable for the handling of the signals including transient phenomena and those with time-variant frequencies like swept frequency which is clarified in this study. Thus, to amend the

*Corresponding author. Email: azadi@kntu.ac.ir

ISSN 0042-3114 print/ISSN 1744-5159 online

DOI: 10.1080/00423110802094298
http://www.informaworld.com

incapability of common methods of vibratory analysis, some authors have suggested using of the wavelet transform (WT) in signal analysis [2,3]. The WT is an analytical method in time-frequency domain which for its potential capability of signal analysis has become a useful tool to detect the local faults and transient phenomena in the dynamic systems in the recent years. In 1994–1999, Newland published various papers in which WT was introduced systematically, and the basic theories and some applications of using wavelet in the signal analysis were also explained [2,4,5].

Onsay used WT to NVH analysis of beams with even cross sections and some kinds of structures to determine the transient response of system vibrations caused by an impulse input [3]. Another study was performed to analyse the noise and vibrations of the shock in the internal combustion engines, using frequency-time transforms such as short-time Fourier transform and WT. These methods also have been applied in processing of random signals (with time-variant frequencies) like a chirp signal that has time-dependent frequencies [6]. Shi *et al.* [7] proposed a new approach based on the fusion of the WT and envelope spectrum for detecting and localising faults in rolling element bearings. Usually in the research studies of the active or the semi-active suspension systems, the closed-loop control systems are used for fault detection. Model-base fault detection and identification methods have been developed in [8,9]. The analytical redundant techniques have been used in [10] for fault detection of active suspension in heavy vehicle. In another study, a passive fault tolerant longitudinal controller was designed for the predefined faults in the public transit [11].

The above-mentioned studies focused on the fault detection of the sensors and the actuators. In this paper, we investigate the defects of passive suspension system parts like damper and upper damper bushing (UDB). The UDB fault modelled as loose joints which are due to incorrect assembly through production process or from wearing, crush or cracking that cause to reduce the bushing stiffness and natural frequency accordingly.

The damper fault appears as the decrease in damping force. In this study, a full vehicle model is simulated by ADAMS/CAR software and the vehicle suspension system (VSS) fault detection investigated by applying swept frequency input to the vehicle. The accelerations of the wheels and body have been analysed based on the continuous wavelet transform (CWT).

The main advantage of the CWT methodology to the spectral analysis is signal frequency contents can be detected more precisely for transient inputs. Obviously, the output signals have transient data and variable frequencies which depend on the time. Commercially, this idea can be applied by automobile manufacturers to offer better customer service after sale. Also it is helpful for improving the quality of technical inspection within a shorter time in assembly line.

2. Continuous wavelet transform

The CWT is based upon a family of functions [12]:

$$\psi_{a,b}(t) = \frac{1}{\sqrt{a}}\psi\left(\frac{t-b}{a}\right), \quad a > b \in \Re \tag{1}$$

where ψ is a fixed function, called the 'mother wavelet', that is localised both in time and frequency. The function $\psi_{a,b}(t)$ is obtained by applying the operations of shifting (b-translation) in the time domain and scaling (a-dilation) in the frequency domain to the mother wavelet [4]. The different wavelets are used for the different purposes. Since the WT is a measurement of similarity between the signal $x(t)$ and a series of the wavelet functions, the suitable wavelet must posses the similar transient characteristic and can be selected to extract the transient features hidden in the signal.

In this paper, the vibration of VSS is a typical exponentially enveloped oscillation signal and can be expressed as:

$$\psi(t) = \mathrm{e}^{-\varsigma t + j2\pi f_r t} \tag{2}$$

where ς and f_r are damping ratio and resonant frequency, respectively [5]. In this attempt, the Morlet wavelet is employed using MATLAB software that $f_o = 0.8125$ Hz is used throughout the mother transformations (f_o is the central frequency of the wavelet) [13].

The CWT of a signal $x(t)$ is defined by:

$$\begin{aligned} W_x^{\psi}(a,b) &= \int_{-\infty}^{\infty} x(t)\psi_{a,b}^*(t)\,\mathrm{d}t \\ &= \frac{1}{\sqrt{a}}\int_{-\infty}^{\infty} x(t)\psi^*\left(\frac{t-b}{a}\right)\mathrm{d}t \end{aligned} \tag{3}$$

where $\psi^*(t)$ is the complex conjugate of $\psi(t)$.

The relationship between signal frequency and scale can be expressed as [13]:

$$f_a = \frac{f_o}{a \cdot \Delta} \tag{4}$$

where f_a is the frequency corresponding to the scale a and Δ is the sampling period [13].

2.1. *Scalogram*

The contribution of signal energy in the specific scale a, and the translation b, is defined by two-dimensional wavelet energy density function known as the scalogram.

$$E(a,b) = \left|W_x^{\psi}(a,b)\right|^2 \tag{5}$$

The total signal energy distribution at a specific a scale is

$$E(a) = \int_{-\infty}^{+\infty} E(a,b)\,\mathrm{d}b \tag{6}$$

The square of the modulus of the CWT can be interpreted as an energy density distribution over the (a, b) time-scale plane. The energy of a signal on this plane is mainly concentrated around the so-scaled ridges of the WT. Extracting the values of the wavelet coefficients through these ridges yields the wavelet skeleton that its real and imaginary components approximate the signal [14].

3. Dynamic modelling of the vehicle

In this section, an off-road vehicle (jeep model) is modelled by ADAMS/CAR software. The rear and front suspension systems are rigid type with helical springs and illustrated in Figures 1 and 2, respectively. The axle 8 is carried by the longitudinal arm 6 and A-type control arms 7 as shown in Figure 1. The A arm absorbs lateral forces and longitudinal arms absorb the drive-off and braking forces. The longitudinal arms are linked to the body and axle by bushing joints. These bushings have translational and rotational stiffness in x, y and z directions. The coil spring 3 and almost vertical shock absorber 4 can be clearly seen in Figure 1.

The steering system is recirculating ball type. The tie rod 5 is modelled like a link and connected to the hob carrier 2 by a spherical joint.

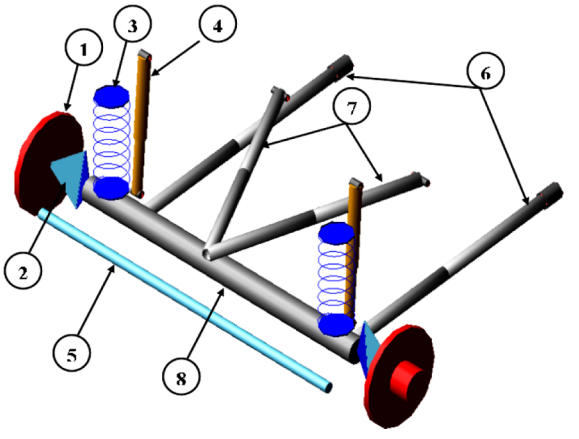

Figure 1. The front suspension system.

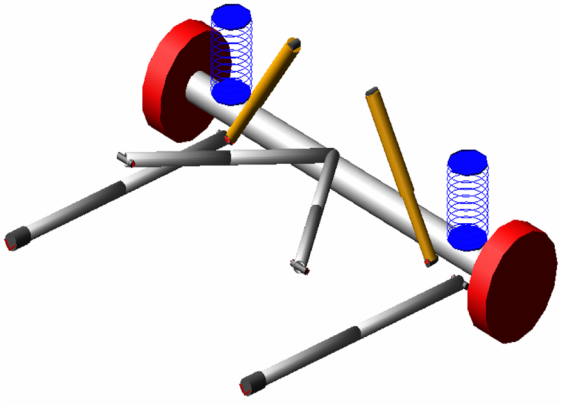

Figure 2. The rear suspension system.

For modelling the steering system, the standard model of Pitman_Arm.tpl in ADAMS has been used. Also a standard template known as Rigid_Chassis.tpl is used to model the body. In this model, the engine, gearbox, fuel tank, spare tyre and other concentrated mass are placed as separate parts, with their masses on the vehicle body. Handling-Tire.tpl is another standard model which is applied to model the tyres.

3.1. *Model validation*

After vehicle dynamic modelling, several 4-post and handling tests run to investigate the handling and ride performances of the vehicle. Then the simulation results were compared with the time history measurements on the vehicle which has been done in the laboratory as shown in Figures 8–12. Some necessary modifications have been made in the model parameters, to get good agreements with the test results. The springs of front suspension are assumed to be linear and their stiffness was equal to 22500 N/m concluded from the static test. In rear suspension, non-linear springs are in use, and the load-deflection diagram is plotted in Figure 3 based on the results from the test bench. The force–velocity characteristics of the front and rear dampers are plotted in Figure 4 which are obtained from dynamic tests. The other vehicle parameters are in Table 1.

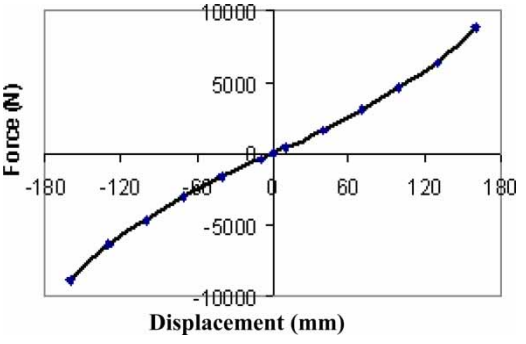

Figure 3. Force *vs* displacement curve for spring of rear suspension.

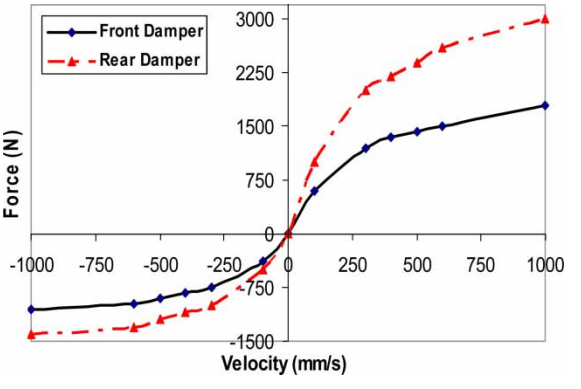

Figure 4. Force *vs* velocity curve for the dampers of front and rear suspension.

Table 1. Full-vehicle model parameters.

Parameter	Value	Parameter	Value
Front suspension stiffness	22500 N/m	Front axle load	790 kg.f
Rear suspension average stiffness	55720 N/m	Rear axle load	900.7 kg.f
Bushings translational stiffness (x or y direction)	45×10^5 N/m	Total vehicle mass	1690.7 kg
		Pitch moment of inertia	1949 kg.m^2
Bushings translational stiffness (z direction)	45×10^4 N/m	Roll moment of inertia	569.2 kg.m^2
		Yaw moment of inertia	2467 kg.m^2
Bushings rotational stiffness (around x or y axis)	45 N.m/deg	Wheel base	2.28 m
		Wheel track (front)	1.48 m
Bushings rotational stiffness (around z axis)	0.8 N.m/deg	Wheel track (rear)	1.47 m

In all cases, very close agreement between test and simulation results were obtained after model updating.

In the laboratory two accelerometer sensors are applied to measure the vertical acceleration: sensor No. 1 (placed on the body, over the front-left part of the wheel) and sensor No. 2 located under the driver's seat. Also optical sensors are employed to measure the pitch and roll angles. The positions of sensors are shown in Figures 5 and 6. The vehicle equipped with the measurement system and the 4-post actuators are shown in Figure 7.

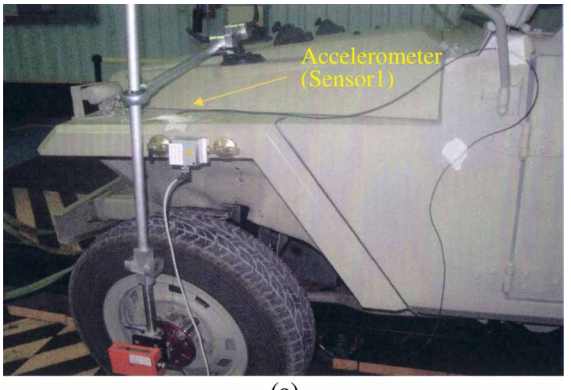

(a)

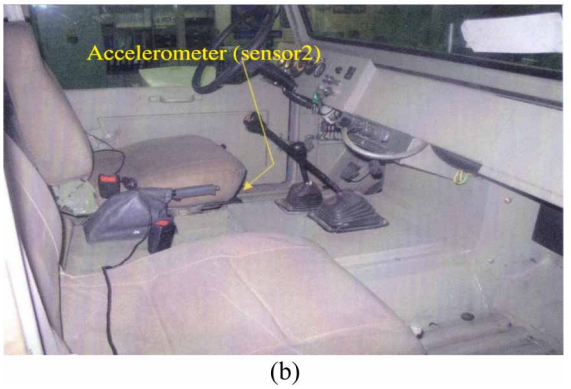

(b)

Figure 5. The accelerometer positions: (a) the position of accelerometer sensor No. 1 and (b) the position of accelerometer sensor No. 2.

Figure 6. Optical sensor for measuring the body roll.

Comparing the results from dynamic simulation and 4-post test as shown in Figures 8– 11 (in these figures the simulation and experimental results have been shown in the figure parts 'a' and 'b,' respectively), revealed an acceptable correspondence between the results in both circumstances of simulation and test. Also in Figure 12 it can be seen the small difference between the vehicle-handling simulation and handling test results. So, the full vehicle dynamic model that is shown in Figure 13 can be verified.

Figure 7. Measuring system in 4-post laboratory.

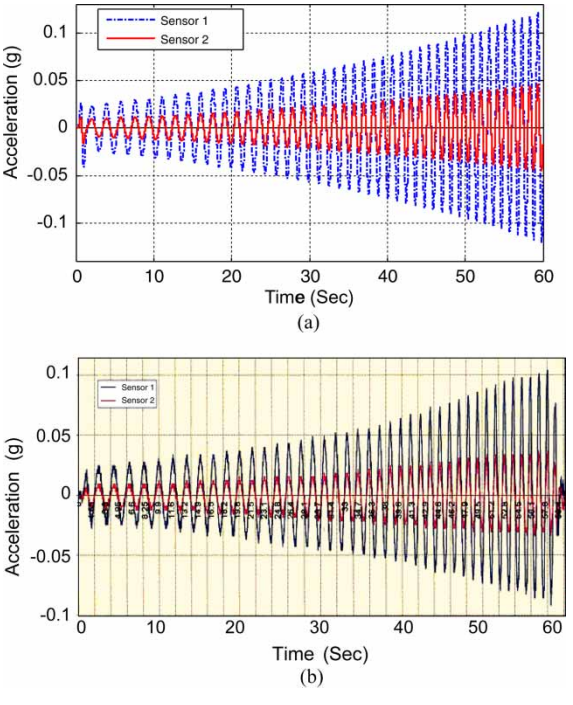

Figure 8. Acceleration responses according to the swept frequency input (0.5–1 Hz and amplitude of 10 mm) applied on front axle: (a) simulation results and (b) experimental results.

As mentioned earlier there are differences in some cases that can be originated from following reasons:

(1) The inflexibility of the vehicle body model (rigidity).
(2) Non-linear dynamic behaviour of spring and dampers due to the contact with bumpers in real state, although these are ignored in modelling.

As mentioned above, in ride performance simulation and in order to choose subsystem, it must be noted that the tyre model is of Delft type and the four wheels are locked by constraints that prevent the forward and backward movements of the vehicle.

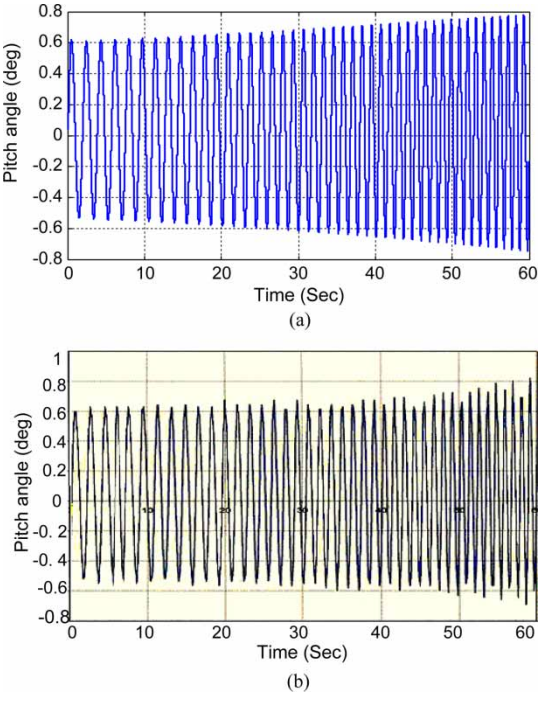

Figure 9. Acceleration responses according to the swept frequency input (0.5–1 Hz and amplitude of 20 mm) applied on rear axle (pitch motion): (a) simulation results and (b) experimental results.

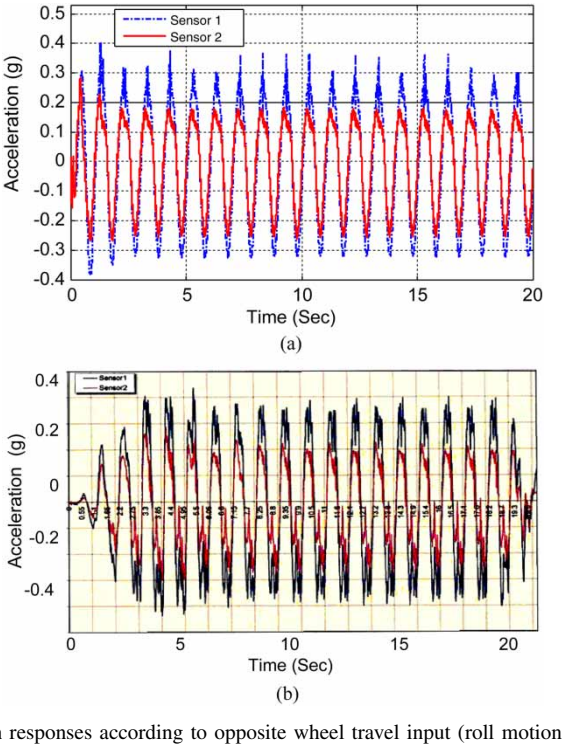

Figure 10. Acceleration responses according to opposite wheel travel input (roll motion 1 Hz and amplitude of 30 mm): (a) simulation results and (b) experimental results.

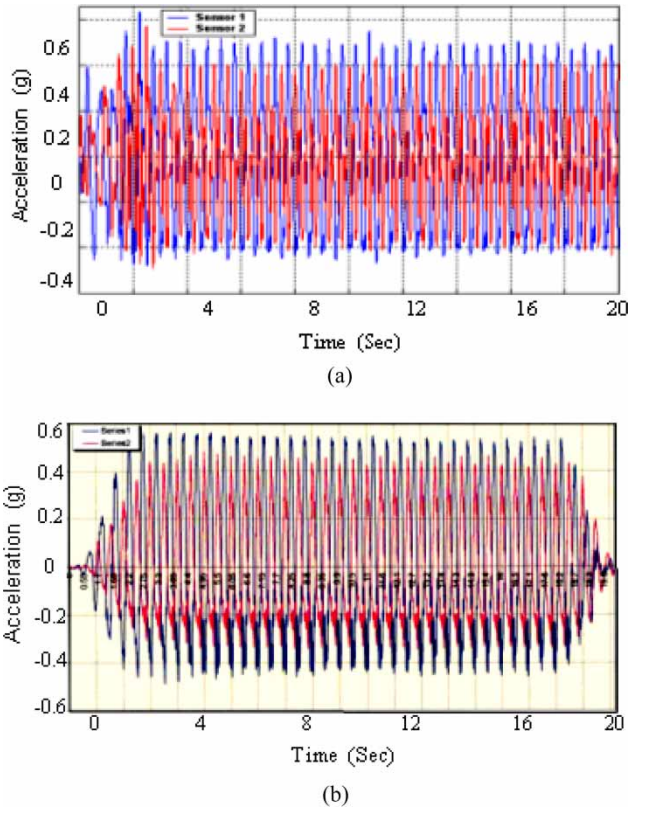

Figure 11. Acceleration responses according to opposite wheel travel input (pitch motion 2 Hz and amplitude of 20 mm): (a) simulation results and (b) experimental results.

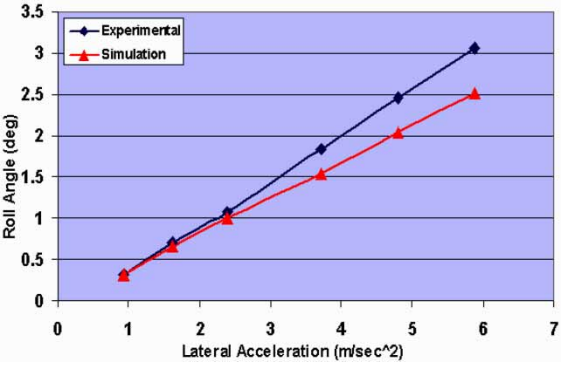

Figure 12. Handling test (roll angle *vs* lateral acceleration, steady state cornering).

4. Signal analyses

In this part, we consider fault-detection in the VSS using the signal energy rate in different frequencies, caused as a result of changing of model parameters. Let us assume that damping force has been decreased about 70% because of damper damage and the clearance of

Figure 13. The full vehicle model in ADAMS.

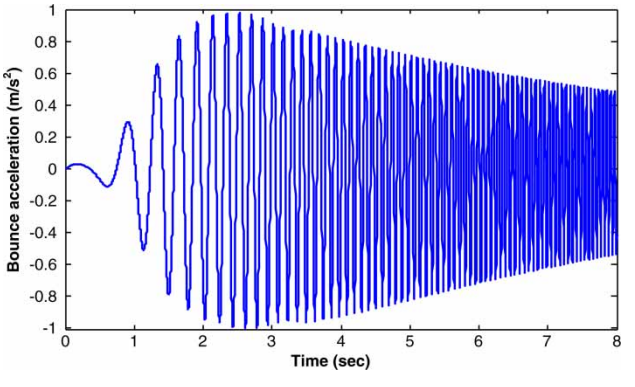

Figure 14. Bounce acceleration (normal damper).

the bushing placed above the front-left damper is 2 mm. The vehicle is exposed to a swept frequency with the constant range of 1.5 mm within 8 s and the frequency range of 0–18 Hz.

At first, we define the spectral analysis weakness to analyse the process of the transient signals containing variable and time-dependent frequencies. In swept frequency signal, the frequency is proportional to variations of time. To calculate PSD, the Hamming window function is employed. As an example, the bounce accelerations in the time domain are illustrated in Figures 14 and 15 that demonstrate the normal and faulty damper, respectively. The PSD transform of these signals are illustrated in Figure 16. In this figure, some oscillations are revealed on PSD curves (especially for higher frequencies in which the transient characteristics of the signals are more intense) and because of that, the accurate diagnosis of pick points are more difficult to estimate and accordingly the difficulty of estimation of natural frequencies. Also, in the time-domain diagrams (Figures 14 and 15), we can see the picks are about 6–6.5 Hz, while in PSD diagram (Figure 16) the pick frequency is nearly 8 Hz. Therefore, the natural frequencies of the system are estimated with large error by spectral analysis.

The high accuracy of wavelet analysis in the process of signals can be observed. Since the WT is defined as a complex value, the signal $x(t)$ should be conveyed in an analytical way in form of $\widehat{x}(t)$. The real part of $\widehat{x}(t)$ is $x(t)$ and the imaginary part is obtained through Hilbert transform of the $x(t)$. Now, the signal frequency contents can be revealed through the energy

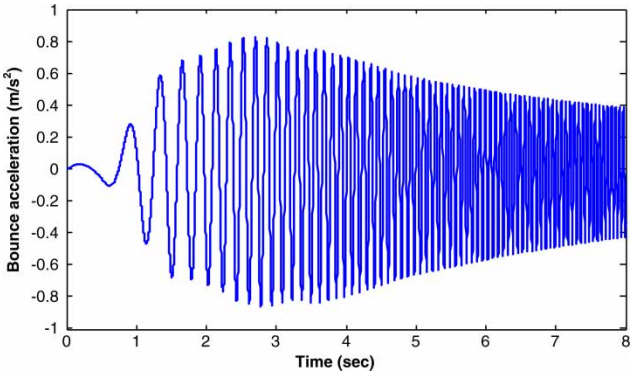

Figure 15. Bounce acceleration (faulty damper).

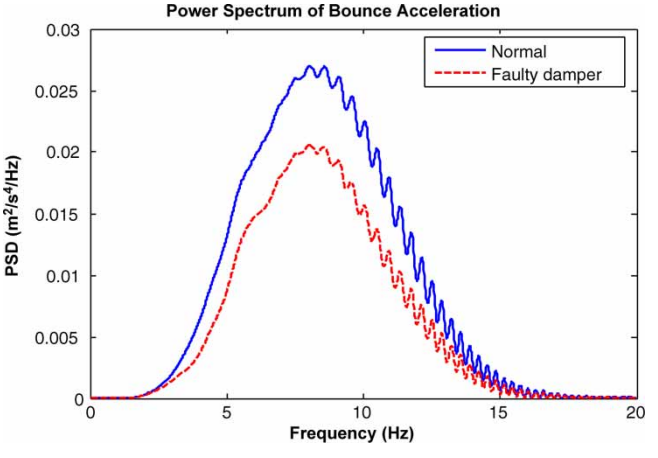

Figure 16. PSD of bounce acceleration for normal and faulty conditions.

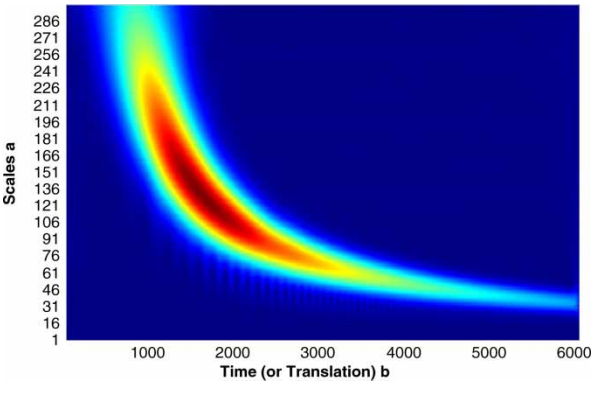

Figure 17. Bounce acceleration WT for normal condition.

distribution of signal in different scales and applying WT, illustrated by $E(a)$. In Figure 17, the time-scale contour of bounce acceleration is illustrated in normal condition.

In this figure, the horizontal axis represents time shifting b in the wavelet analysis and can be obtained by definition of a dimensionless coefficient 1 HZ/f_{samp}, where f_{samp} is the sampling frequency. Considering this fact that the signal sampling frequency has been 750 Hz, then the

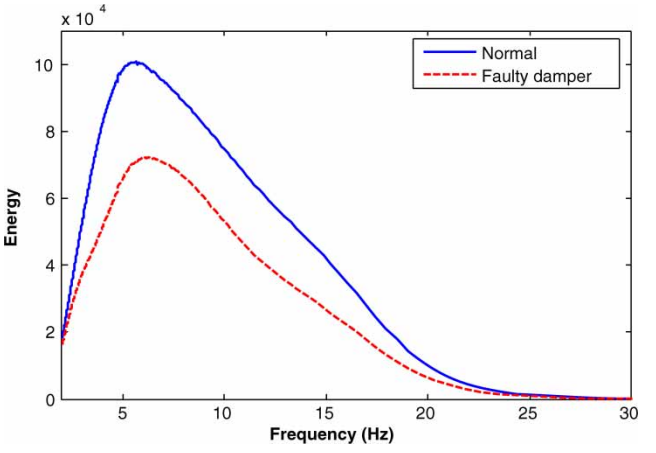

Figure 18. Bounce acceleration energy distribution using CWT.

dimensionless coefficient will be 0.00133. Thus, the relation between b and time t can be stated as follows:

$$t = 1.33 \times 10^{-3} \cdot b \tag{7}$$

For example, from Equation (7) the final b, b_{fin}, can be obtained through the final time ($t_{\text{fin}} = 8$ s, $b_{\text{fin}} = 8/0.00133 = 6000$).

In Figure 17, a dominant frequency is revealed as centre of light contour. For this signal the energy diagram $E(a)$ is illustrated in Figure 18 to determine the accurate value of dominant frequency. The signal energy distribution related to faulty damper can also be observed in this figure. According to Figure 18, the pick frequency in bounce acceleration signal is 6 Hz using the wavelet analysis, while the value of about 8 Hz can be obtained from the curve of Figure 17. Equation (4) applied to calculate the corresponding frequency in any scale such that the scale frequency can be substituted for the values concerning the horizontal axis of diagram 19.

Thus, the faults developed in the suspension system can be diagnosed more accurately using signal energy distribution through applying CWT. In this paper, it is assumed that the faults of damper and bushing are in the front-left part of the suspension system; to see the changes made as a consequence, the acceleration signals of the four wheels have been studied in three steps which are:

(1) The system in normal condition.
(2) The damper is faulty.
(3) The bushing is faulty.

The energy contents $E(a)$ of the wheels' bounce acceleration are shown in Figure 19a–d using CWT. By comparison with these figures, generally it is shown that the increase in energy is a result of fault in the system and if one of the front wheels is faulty, no significant change will be seen in the energy of rear wheels. Also the following results conveyed in more details.

Figure 19a shows the bounce acceleration of the front-left wheel in these three steps. The natural frequency of the un-sprung mass revealed as a peak has the value of 13.5 Hz when it is normal. The decrease of the damping force in the damper and clearance of bushing has led to decrease of peak frequency to 10.9 and 10.5 Hz, respectively. Also it is caused to increase the energy concerning the frequencies 3 and 1.7 times, respectively, as a result of the faults.

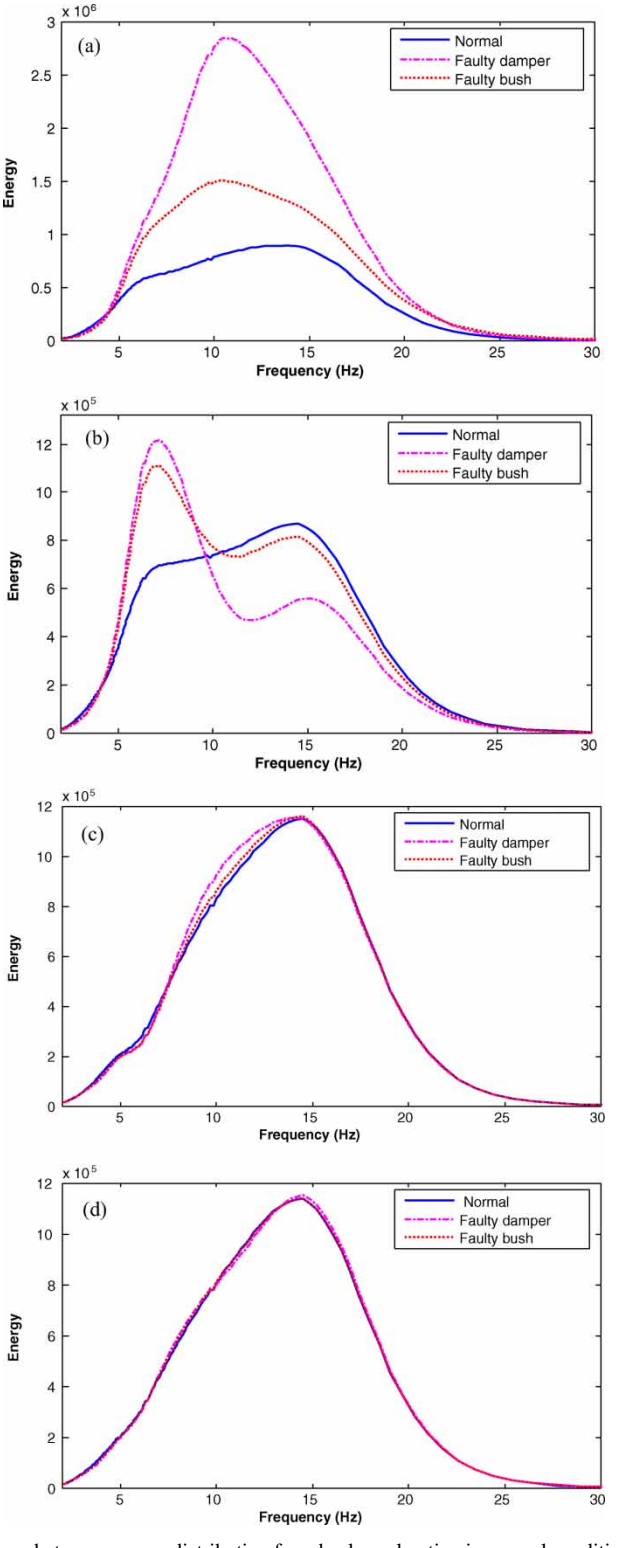

Figure 19. Comparison between energy distribution for wheel acceleration in normal condition, faulty damper and faulty bushing: (a) front-left; (b) front-right; (c) rear-left and (d) rear-right.

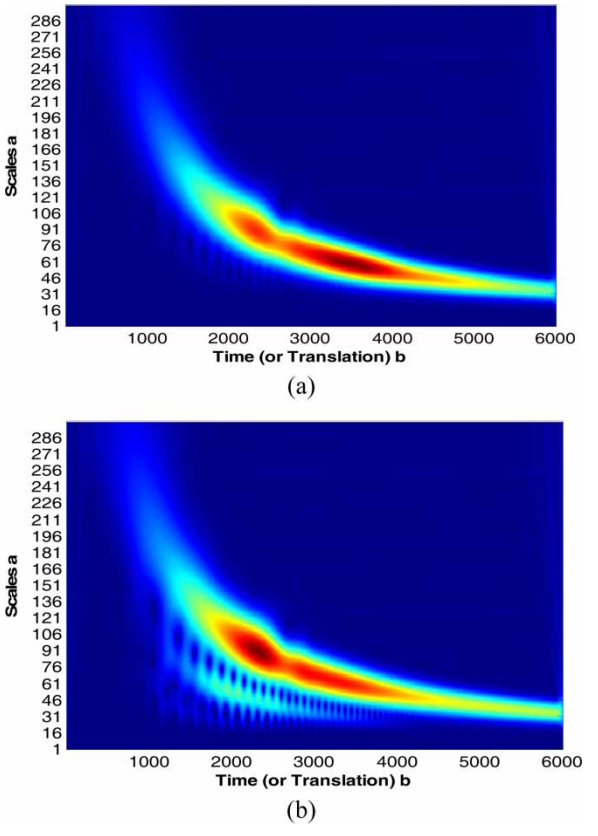

Figure 20. Wavelet transform of the front-left wheel acceleration: (a) faulty damper and (b) faulty bushing.

The bounce acceleration of the front-right wheel is shown in Figure 19b. The peak frequencies of a normal system have the values of 7.5 and 14.5 Hz. No significant changes have been found in the values of these two frequencies concerning the faults of bushing and damper, but there are some changes in the amount of energy in these peak frequencies.

In Figure 19c and d which concern the acceleration of rear-left and right wheels, respectively, no significant changes are visible in all cases.

Thus, significant changes of the peak frequency (that is pertinent to the natural frequency of un-sprung mass) can be seen in the faulty part (front-left part) and the signal energy of the wheel bounce acceleration, significantly, increase. So, it is easy to detect the faulty suspension among the other suspensions.

Now, to study the mechanism of the fault arising from bushing and damper, the time-scale contours of CWT coefficient for the front-left wheel acceleration, illustrated in Figure 20a and b, respectively.

When the bushing is faulty, besides a light strip is visible in contour that shows the signal frequency contents, another frequency with the scale of 60 (10.5 Hz) is revealed in a lower peak 7.5 Hz in resonant frequency of the body. In order to determine this scale accurately, it is better to use the signal energy distribution, $E(a)$, up to $b = 2000$ (42% of the total time interval) in Figure 21. The above-mentioned peak of 52 (11.71 Hz) would be observed when zoom in on this diagram. This frequency can be pertinent to the natural frequency of un-sprung mass of front-left suspension. Moreover, it decreases from 13.5 Hz, when the bushing is normal, to

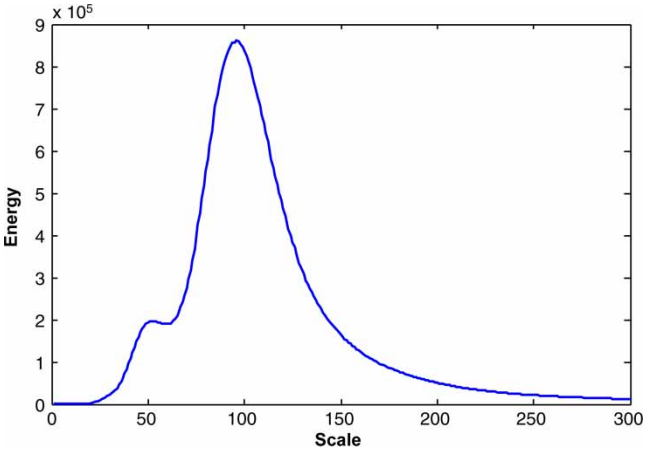

Figure 21. Energy distribution of front-left wheel acceleration with faulty bushing ($t = 0 - 3.33$ s).

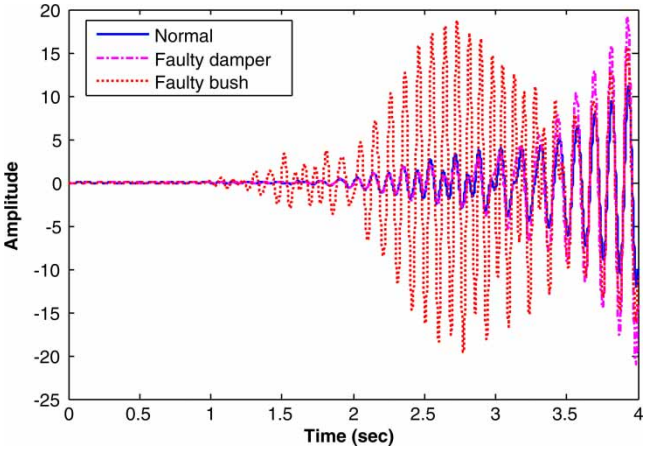

Figure 22. Comparison between normal system, faulty damper and faulty bushing for the skeleton plot of front-left wheel acceleration.

11.71 Hz, when the bushing has loose joints or damaged. Evidently, to study the authenticity of this conclusion may need more detailed researches on the subject of non-linear vibrations.

To make this phenomenon clear, the skeletons of CWT coefficients in the scale of 52 has been illustrated in Figure 22 for interval of 4 s.

Within 2.75 s the body natural frequency has resonance, and this frequency shows up more intensively compared with the other two conditions. In other words, only in this state, when the time is near to 2.75 s, the frequency has a relative maximum point. Therefore, the faulty UDB is distinguished from faulty damper.

5. Conclusions

The paper presented a methodology for analysis of the signals containing transient data or frequency–time dependent for fault detection of VSS. It has shown that the spectral analysis cannot reveal the frequency contents of such signals. On the contrary, using energy distribution

in different frequencies, and employing WT to this type of signal can be analysed in a shorter time and more accurately. Thus, in such cases, if WT is employed for fault detection of VSS, the required time to apply input can be decreased to a certain limit and with high-precision estimation of system natural frequencies.

Defects of damper and bushing of one suspension does not make any changes in the natural frequencies of the un-sprung mass of the other suspensions, but it decreases the natural frequencies of the same faulty suspension.

Commercially, this method not only detects the faults of VSS in assembly line but also can be used by automobile manufacturers to offer better customer service after sale.

Acknowledgements

The authors are grateful to the referees for valuable comments on this paper and technical support of the vehicle research department engineers.

References

[1] P.D. McFadden, *Condition monitoring of rolling element bearing by vibration analysis*, in *Machine Condition Monitoring*, Institute of Mechanical Engineers, London, 1990, pp. 46–54.
[2] D.E. Newland, *Wavelet analysis of vibration. 1. Theory*, J. Vib. Acoust. 116 (1994), pp. 409–416.
[3] T. Onsay, *The use of wavelet transform and frames in NVH applications*, SAE 951364, 1995, pp. 1057–1068.
[4] D.E. Newland, *Wavelet analysis of vibration. 2. Wavelet maps*, J. Vib. Acoust. 116 (1994), pp. 417–425.
[5] D.E. Newland, *Ridge and phase identification in the frequency analysis of transient signals by harmonic wavelet*, J. Vib. Acoust. 121 (1999), pp. 149–155.
[6] I.S. Suh, *Application of time-frequency representation techniques to the impact-induced noise and vibration from engines*, SAE 01-0453, 2002.
[7] D.F. Shi, W.J. Wang, and L.S. Qu, *Defect detection for bearings using envelope spectra of wavelet transform*, J. Vib. Acoust. 126 (2004), pp. 567–573.
[8] D. Fischer, E. Kaus, and R. Isermann, *Fault detection for an active vehicle suspension*, in *American Control Conference Proceedings*, Vol. 5, 4–6 June 2003, pp. 4377–4382.
[9] M. Borner, H. Straky, T. Weispfenning, and R. Isermann, *Model based fault detection of vehicle suspension and hydraulic brake systems*, Mechatronics 12 (2002), pp. 999–1010.
[10] B.P. Jeppesen and D. Cebon, *Analytical redundancy techniques for fault detection in an active heavy vehicle suspension*, Sixth International Symposium on Advanced Vehicle Control, AVEC 2002, Hiroshima, Japan, September 2002.
[11] B. Song, K.J. Hedrick, and A. Howell, *Fault tolerant control and classification for longitudinal vehicle control*, Trans. ASME 125 (2003), pp. 320–329.
[12] S.K. Lee and P.R. White, *Application of wavelet analysis to the impact harshness of a vehicle*, Proc. IMechE, Part C 214 (2000), pp. 1331–1338.
[13] MATLAB Software, Version 7, Wavelet Toolbox Help.
[14] W.J. Staszewski, *Analysis of non-linear systems using wavelets*, Proc. IMechE, Part C 214 (2000), pp. 1339–1353.